RM E54G26

NACA

RESEARCH MEMORANDUM

PRELIMINARY INVESTIGATION OF AN ASYMMETRIC SWEPT NOSE INLET OF CIRCULAR PROJECTION AT MACH NUMBER 3.85

By James F. Connors and Richard R. Woollett

Lewis Flight Propulsion Laboratory
Cleveland, Ohio

NATIONAL ADVISORY COMMITTEE FOR AERONAUTICS

WASHINGTON

October 11, 1954
Declassified October 16, 1961

NATIONAL ADVISORY COMMITTEE FOR AERONAUTICS

RESEARCH MEMORANDUM

PRELIMINARY INVESTIGATION OF AN ASYMMETRIC SWEPT NOSE INLET OF CIRCULAR PROJECTION AT MACH NUMBER 3.85

By James F. Connors and Richard R. Woollett

SUMMARY

A preliminary experimental investigation of the performance capabilities of an asymmetric swept nose inlet of circular projection has been conducted in the Lewis 2- by 2-foot supersonic wind tunnel at a Mach number of 3.85. Designed primarily to maintain high performance at angle of attack, the asymmetric inlet was evaluated in terms of its pressure recovery and mass-flow characteristics for angles of attack up to 9°. The performance of this inlet was compared with that previously reported for the more conventional, axially symmetric, annular nose inlets.

At zero angle of attack, the asymmetric swept nose inlet indicated a total-pressure recovery of 0.40 at a corresponding mass-flow ratio of 0.96. With an increase in angle of attack to 9°, maximum mass-flow ratio and critical pressure recovery increased to 1.075 and 0.41, respectively. This inlet exhibited subcritical flow stability at angle of attack and good velocity profiles at the diffuser exit under all operating conditions. Its angle-of-attack characteristics were thus superior to those of the axially symmetric, annular nose inlets previously reported. In addition, the asymmetric inlet appears to be a potentially low-cowl-pressure-drag configuration.

INTRODUCTION

Recent experimental studies by the NACA on axially symmetric, annular nose inlets at Mach number 3.85 (refs. 1 and 2) have indicated that all annular nose inlets exhibit a decrease in both critical pressure recovery and maximum mass flow with increasing angle of attack. These low Reynolds number studies showed that centerbody crossflow effects resulted in a boundary-layer thickening on the top or lee side of the spikes. In some cases (for the 2-cone and isentropic inlets), complete separation of the flow from the top of the spikes was encountered at angles of attack less than 9°. In addition, the increased compression on the under side of

the spike at angle of attack was more than offset by the decreased compression on the top side. Sensitivity to these effects increased with the higher-compression inlets and was most pronounced for the isentropic inlets.

For improved internal-flow performance at angle of attack, the design of a new inlet geometry was directed toward eliminating adverse boundary-layer cross-flow effects and nonuniform compression at the entrance. In addition, it was desired to obtain a low cowl pressure drag and a cylindrical external housing for ease in fairing to circular engines. The resulting design (fig. 1(e)) had no central body and utilized a sweptback leading edge with an asymmetric compression surface located in the upper half of the inlet. Since the leading-edge sweep allowed for flow spillage up to the minimum area for starting, the asymmetric inlet utilized effectively all-external supersonic compression. For high pressure recoveries, smooth continuously curved compression surfaces were employed. A characteristic of this asymmetric swept nose inlet was that with increasing angle of attack there was an attendant increase in both the projected capture area and the degree of compressive flow turning.

An inlet similar in some respects to the present asymmetric swept nose inlet is proposed in reference 3. This inlet was derived from a known axisymmetric flow; however, it employed large amounts of internal contraction.

The purpose of this present investigation is to demonstrate experimentally the performance capabilities of an asymmetric swept nose inlet at Mach number 3.85, to compare its results with those of conventional annular nose inlets (ref. 2), and to indicate possible contour-design criteria based on the results of these exploratory tests. Performance evaluations are based on pressure recovery and mass-flow characteristics over an angle-of-attack range from -3° to 9°.

SYMBOLS

The following symbols are used in this report:

M Mach number

m_0 maximum mass-flow rate through free-stream tube equal in area to maximum inlet capture area at $\alpha = 0^\circ$, $\frac{\pi}{4}(3.62)^2$ sq in.

m_3 mass-flow rate passing into inlet

P total pressure, lb/sq ft

R wall radius at diffuser exit (1.80 in.)

r local radius at diffuser exit, in.

α angle of attack, deg

Subscripts:

0 free-stream conditions

3 conditions at diffuser exit

APPARATUS AND PROCEDURE

The experimental investigation was conducted in the NACA Lewis 2- by 2-foot supersonic wind tunnel, which was operated at a Mach number of 3.85 and a simulated pressure altitude of approximately 105,000 feet. The tunnel air was maintained at a stagnation temperature of $200^{\circ}\pm5^{\circ}$ F and at a dew-point temperature of $-20^{\circ}\pm5^{\circ}$ F. Based on the maximum cowl diameter (3.85 in.), the test Reynolds number was approximately 330,000.

A schematic drawing of the model installed in the tunnel test chamber is shown in figure 1(a). At the exit of the model, an adjustable plug was used to vary the sonic discharge area and, at the same time, the diffuser back pressure. The tunnel strut assembly supported the model and permitted angle-of-attack variations up to 9°.

There were three configurations of the asymmetric swept nose inlet, each involving a variation in the compression-surface contouring. These were designated as configurations A, B, and C, with A being the initial version. Design and fabrication details are given in the drawings of figures 1(b), (c), and (d).

In the design of the initial contours of configuration A, there appeared to be no adequate theoretical approach readily available for prescribing the ideal inlet shape. Consequently, somewhat crude approximations were employed in order to arrive at the initial geometry. The axial center-line contour (fig. 1(b)) was assumed to be a two-dimensional reverse Prandtl-Meyer streamline with the flow being compressed down to a Mach number of 1.75. The leading edge of the inlet was swept back at the initial shock angle of 22°. At the axial stations, corresponding to the templates on the drawing, an average Mach number was determined from an area-weighted integration across the assumed two-dimensional center-line characteristics. From these Mach numbers and the isentropic area relations, an area variation was derived as a function of axial distance. Then, at each station, contours were worked out to satisfy the above conditions, that is, two fixed points given by the intersection of the swept leading edge with the free-stream tube, a third point given

by the assumed center-line contour, and, finally, a flow area. For more than half the distance (up through station 5.79 in.) from the tip, the area was approximated by cross-sectional circular-arc contours. Reference 3 served as a partial guide in attempting to maintain somewhat similar cross sections while, at the same time, satisfying the area requirements. Beyond station 5.79 inches, a circular arc was unsatisfactory and a distortion of the contours was required to meet the area needs up to the throat. The subsonic portion of the diffuser incorporated an axial area distribution equivalent to that of a straight 5° conical area expansion.

Modifications to this initial inlet geometry were made to form configurations B and C. The contours of configuration B (fig. 1(c)), although quite arbitrary, were directed toward achieving an increase in zero-angle-of-attack mass flow above that realized with configuration A. Compared with configuration A, this geometry approximated more closely a two-dimensional compression surface with a smaller degree of turning along the center line and a larger throat area. The contour modifications for configuration C (fig. 1(d)) were aimed at increased compression above that obtained for configuration B. The cross-sectional shapes were quite similar to those of configuration B up through station 7. From station 7 to the throat, the center portion of the compression-surface cross section became more and more convex. For configuration C, the center-line contour was the same as the two-dimensional streamline contour of configuration A. The direction of compression-surface modifications, then, tended to proceed in some degree from concave cross sections (configuration A), to essentially flat cross sections (configuration B), and finally to convex cross sections (configuration C).

Details of the fabrication techniques are illustrated in the drawing of figure 1(b). The model was made in two parts, an outer steel casing common to all configurations and an inner casting. The material used in the center casting was a low-melting-point alloy of tin and bismuth, which was particularly good because of the ease with which it could be cold-worked into the desired contours. For most modifications, manual scraping was sufficient. A photograph and a sketch of configuration C are presented in figure 1(e).

Instrumentation consisted of a (40-tube) total-pressure rake, four rake static-pressure tubes, and four wall static-pressure orifices, all located in the measuring plane at the diffuser exit as indicated in the sketch of figure 1(a). Pressures were indicated on a multitube differential manometer board with tetrabromoethane as the working fluid. For visual flow observations, a twin-mirror schlieren system was used with either steady or 1-microsecond exposure times.

The total pressures at the diffuser exit were calculated by an area-weighted integration of the local rake pressures. Mass-flow

calculations were based on the measured static pressure at the diffuser exit and the sonic discharge area. For a calibration of the mass-flow measuring system, a 1-cone axially symmetric nose inlet having the initial tip shock passing well inside the cowl with no flow spillage was used.

Complete data were recorded over a wide range of exit-plug positions for angles of attack from -3° to 9°. Configuration C was also investigated at 3° angle of yaw.

RESULTS AND DISCUSSION

Diffuser performance characteristics of the various asymmetric swept nose inlets are presented in figure 2. For configuration A (fig. 2(a)), the critical pressure recovery was 0.395 at zero angle of attack and remained approximately constant up through 9° angle of attack. Supercritical mass-flow ratio, however, was quite low (0.715) at zero angle of attack, increased to a maximum (0.885) at 3°, and then dropped off again with further increases in angle of attack. At each attitude of the inlet, there was an appreciable range of subcritical flow stability. In general, the subcritical pressure recoveries were higher than the critical value at angle of attack. Obviously, the main objection to this particular configuration would be its excessive supercritical mass-flow spillage at zero angle of attack.

As shown by the data of figure 2(b), the modification in contour to configuration B produced a much higher supercritical mass-flow ratio (0.98) at zero angle of attack. However, there was an attendant decrease in both subcritical flow stability and critical pressure recovery (down to 0.34). At angle of attack a maximum mass-flow ratio of 1.18 was attained at 6°. This 20-percent increase in mass flow with 6° angle of attack was accomplished primarily as a result of a concomitant 25-percent increase in projected capture area of the inlet. In general, the critical pressure recovery increased with angle of attack to approximately 0.40 at $\alpha = 9^{\circ}$. Again there was some subcritical stability at each angle of attack. At 3° and 6°, there was a slight localized oscillation of the shock in the vicinity of the lip which appeared particularly sensitive to the positive slope criterion (ref. 4) for inlet buzz conditions. An objective of further modifications to the compression-surface contours was to increase the level of zero-angle-of-attack pressure recovery.

The performance characteristics of configuration C are presented in figure 2(c). At zero angle of attack, a critical pressure recovery of 0.40 was attained at a mass-flow ratio of 0.96. Both critical pressure recovery and supercritical mass-flow ratio increased with angle of attack to values of 0.41 and 1.075, respectively, at 9°. At each positive angle of attack, there was a pronounced subcritical stability range. Also

included on the figure are the diffuser characteristics, showing a drop-off in performance, for 3° negative angle of attack and also for 3° angle of yaw.

The supercritical flow patterns obtained with the asymmetric swept nose inlets, configurations A, B, and C, are illustrated by the schlieren photographs of figures 3(a), (b), and (c), respectively. In each case at zero angle of attack, a strong bow-shock formation stood ahead of the downstream lip surface. With increasing angle of attack, the bow shock moved progressively further upstream of the entrance. The projection of this bow wave ahead of the lip does not necessarily indicate large flow spillage, since observation of the flow was made across a station where the local spillage was apt to be greatest and which represented only a small portion of the periphery of the free-stream tube of entering air.

The oblique shocks emanating from the compression surfaces were, for configuration A, located well out ahead of the swept leading edge. This pattern was indicative of probable large amounts of flow spillage over the sides, which could explain the resulting low mass-flow ratios obtained with this particular inlet. The patterns for configurations B and C at zero angle of attack were quite similar and showed the oblique shocks falling very close to the swept leading edge. At angle of attack, however, the patterns for configuration C, unlike those for configuration B, showed the vortex sheets passing outside of the inlet, thereby accounting for the lower mass-flow ratios obtained with this geometry as compared with that for configuration B.

Additional flow patterns obtained with configuration C are presented for the following conditions: supercritical flow at 3° negative angle of attack (fig. 4(a)), minimum stable mass-flow ratio at 9° angle of attack (fig. 4(b)), and a typical buzz condition at zero angle of attack with a 1-microsecond exposure time (fig. 4(c)). With subcritical stability, there was no significant change from the supercritical pattern, except that the bow wave was positioned further upstream from the lip. The buzz pattern shows the influence of the inlet disturbance in its extreme forward position. Separation of the flow extended all the way forward to the tip of the inlet. At the other extreme of the pulse cycle, the minimum stable mass-flow pattern appeared to be reestablished. Unlike the axisymmetric inlets of reference 2, which had no subcritical stability at all, the asymmetric swept nose inlets did operate stably for limited ranges at reduced mass flow.

The subcritical stability ranges obtained with configuration C at the various angles of attack are further illustrated by the data of figure 5, actually a cross plot of figure 2(c). Designated by the cross-hatched area, the stable range was relatively small (approximately 2 percent) at zero angle of attack and appreciable (approximately 20 percent) at 6° to 9° angles of attack. In each case the pressure recovery

increased slightly with reduced mass flow. The maximum pressure recovery (0.47) was attained at 9° angle of attack at the minimum stable mass-flow ratio (0.875). No subcritical stability was obtained at negative angle of attack or at angle of yaw at zero angle of attack.

Mach number profiles across the diffuser exit are presented in figure 6 for configuration C. Exceptionally good, uniform profiles were obtained throughout the entire test range, even at 9° angle of attack and with the flow well supercritical. This is in contrast to the separated profiles for $\alpha \geq 3^\circ$ obtained with the axisymmetric inlets of reference 1. A factor associated with the attainment of such uniform exit-velocity distributions may well be the location of a strong bow shock ahead of the entrance (or minimum area) at all times. In such a condition the asymmetric inlet operates with a subsonic entrance flow and, during supercritical operation, has a secondary diffuser shock of a strength considerably lower than would be the case for its counterpart with supersonic entrance flow. Thus, the tendency towards profile distortions or flow separations due to local high adverse pressure gradients would be minimized. In the profiles of figure 6 there were no indications whatsoever of separation.

In figure 7, a comparison based on total-pressure recovery and capture mass flow is made between the asymmetric-swept nose inlets and the more conventional axially symmetric annular inlets of reference 2. The performance curves of the three asymmetric configurations are merely cross plots of data from figure 2. The results of configuration C were considered to be most representative of the type of performance attainable with the asymmetric inlet geometry and will be the values referred to in the subsequent comparisons. At zero angle of attack, the critical pressure recovery and the maximum mass-flow ratio of the asymmetric inlet compared quite well with the values for the 2-cone (tip roughness) inlet. At 9° angle of attack, the asymmetric inlet had a 25-percent greater mass flow and a 14-percent higher pressure recovery than the corresponding values for the 2-cone inlet. With the asymmetric inlet, mass flow and critical pressure recovery (to a slight degree) increased with increasing angle of attack and thus indicated superior angle-of-attack characteristics.

The asymmetric swept nose inlet also appears to be potentially a low-cowl-pressure-drag configuration. The cowl frontal area on which the pressures must act is a maximum at one point on the circumference (see point X, fig. 1(b)) and goes to zero on the opposite side. At the same time the fairing from the swept leading edge to the maximum body diameter rapidly decreases the external cowl angle to further reduce the drag. Thus, although the cowl pressures are probably large locally at the point of maximum lip angle, the integrated drag may be relatively small.

In order to eliminate the one-directional drawback to this type of inlet, a variable-geometry arrangement may be feasible. For application

to aircraft operating over a wide range of attitudes, the asymmetric swept nose inlet, due to its cylindrical external form, could be made adjustable in rotation. As such, it would be maintained at zero or positive angle of attack relative to the air stream at all times regardless of the attitude of the aircraft proper. However, there also may be fixed-geometry applications of this inlet wherein one-directional operation may be satisfactory.

It is believed that the demonstrated performance of the asymmetric swept nose inlet is of sufficient merit to warrant further developmental research. There exists a need for the establishment of further design criteria relating to the optimization of the compression-surface contours in order to more adequately prescribe a design procedure. Also, experimental verification of the low-drag potentialities of this type of inlet should be obtained through actual force measurements.

SUMMARY OF RESULTS

A preliminary investigation at Mach number of 3.85 has been conducted in the 2- by 2-foot supersonic wind tunnel on an asymmetric swept nose inlet of circular projection. This inlet, designed primarily to maintain high performance at angle of attack, yielded the following results:

1. At zero angle of attack, the asymmetric swept nose inlet indicated a total-pressure recovery of 0.40 at a corresponding mass-flow ratio of 0.96.

2. With increasing angle of attack to 9°, the pressure recovery and the mass-flow ratio increased to values of 0.41 and 1.075, respectively. In general, the angle-of-attack characteristics of the asymmetric swept nose inlet appeared superior to that of the axially symmetric annular nose inlet.

3. Additional performance characteristics of the asymmetric inlet included subcritical flow stability at angle of attack and good velocity profiles at the diffuser exit under all operating conditions.

Lewis Flight Propulsion Laboratory
National Advisory Committee for Aeronautics
Cleveland, Ohio, July 21, 1954

REFERENCES

1. Connors, James F., and Woollett, Richard R.: Performance Characteristics of Several Types of Axially Symmetric Nose Inlets at Mach Number 3.85. NACA RM E52I15, 1952.

2. Connors, James F., and Woollett, Richard R.: Force, Moment, and Pressure Characteristics of Several Annular Nose Inlets at Mach Number 3.85. NACA RM E53J09, 1954.

3. Evvard, John C., and Maslen, Stephen H.: Three-Dimensional Supersonic Nozzles and Inlets of Arbitrary Exit Cross Section. NACA TN 2688, 1952.

4. Sterbentz, William H., and Evvard, John C.: Criterions for Prediction and Control of Ram-Jet Flow Pulsations. NACA RM E51C27, 1951.

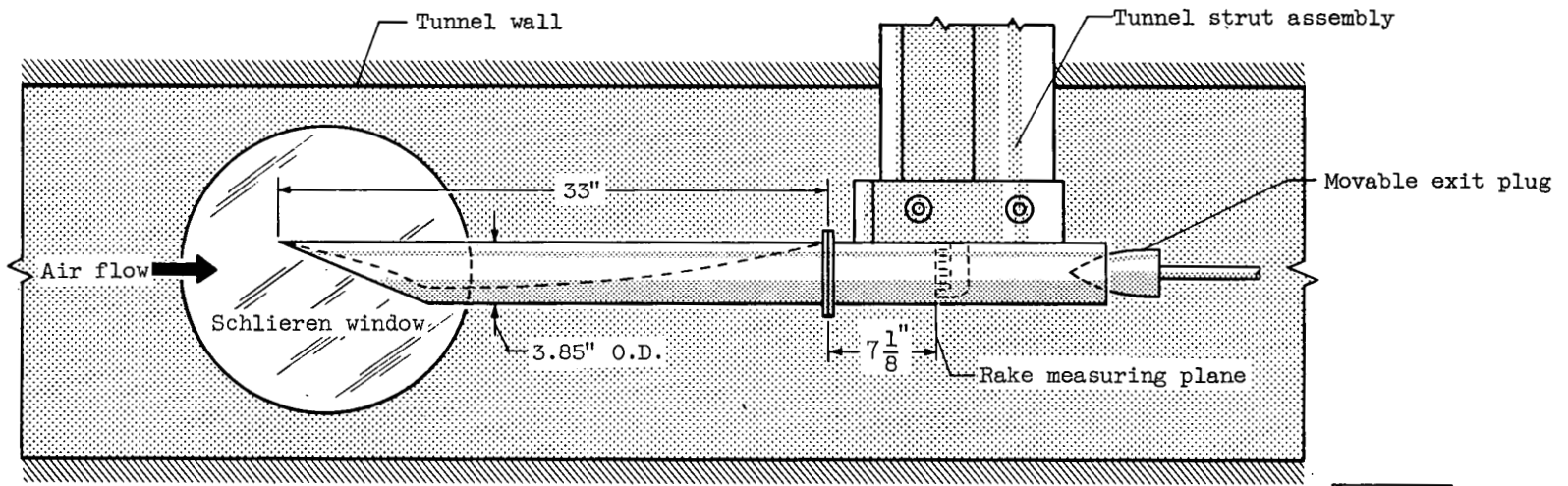

(a) Schematic drawing of model installation in 2- by 2-foot supersonic wind tunnel.

Figure 1. - Experimental apparatus.

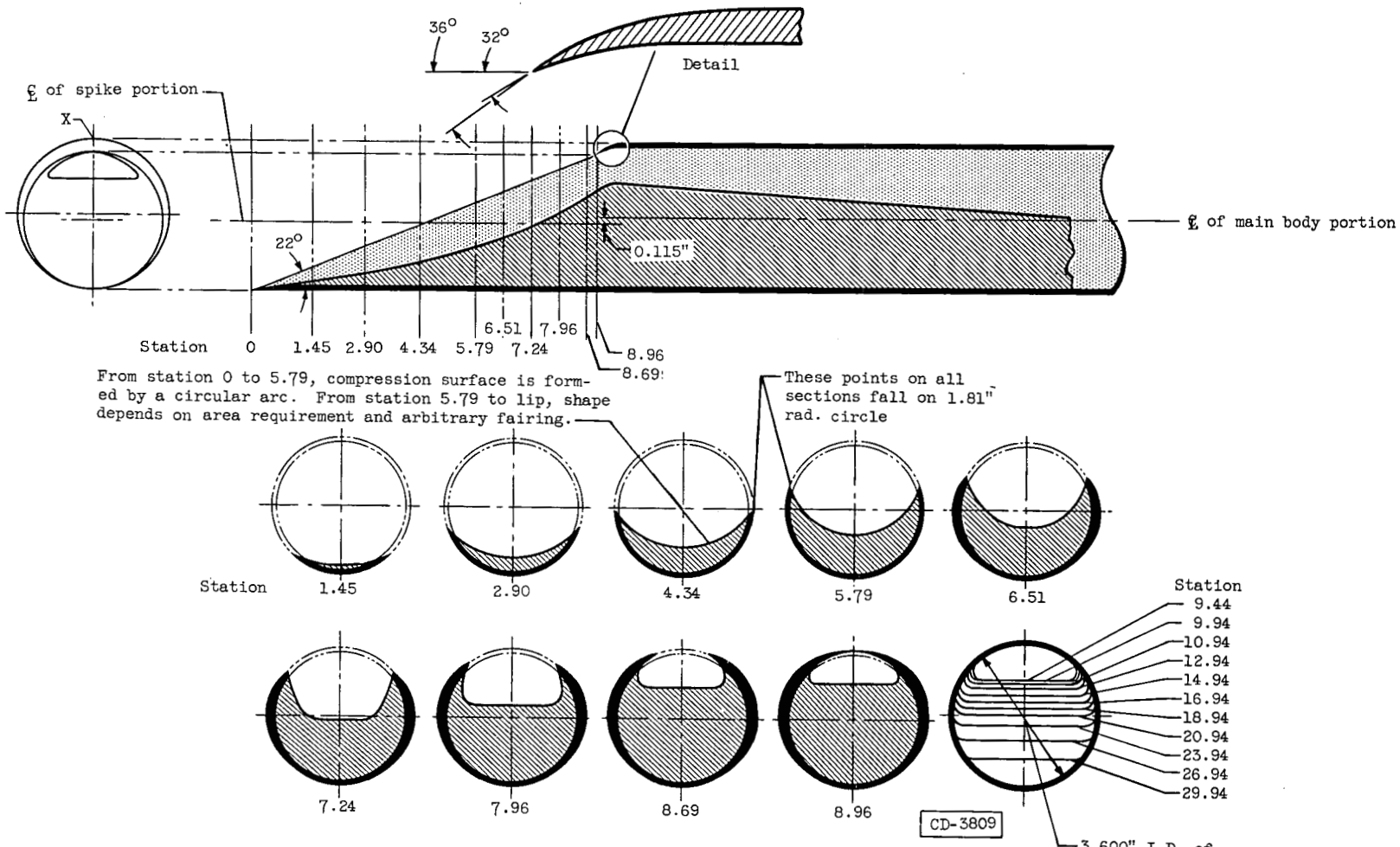

(b) Design details of asymmetric nose inlet, configuration A.

Figure 1. - Continued. Experimental apparatus.

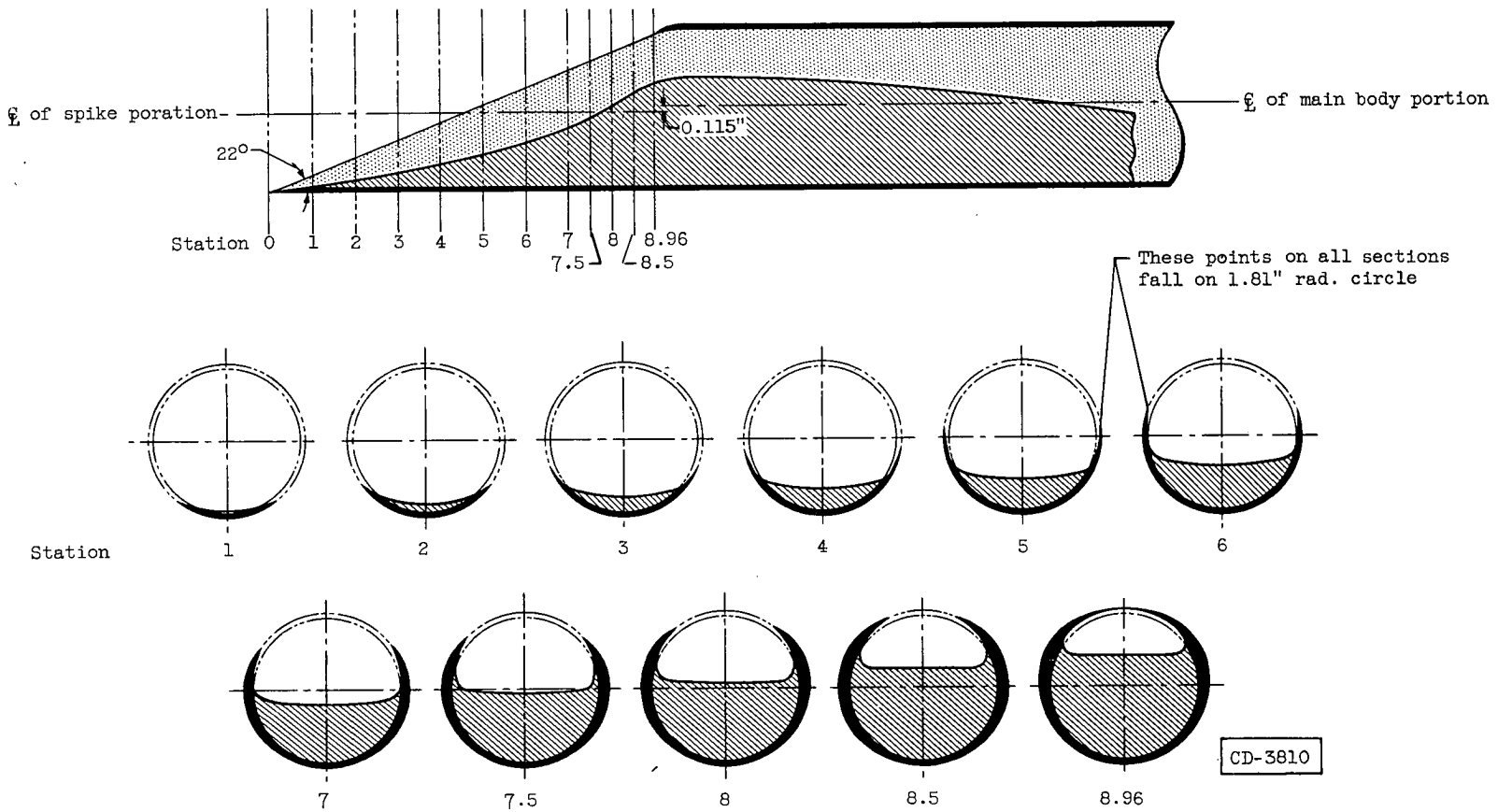

(c) Design details of asymmetric nose inlet, configuration B.

Figure 1. - Continued. Experimental apparatus.

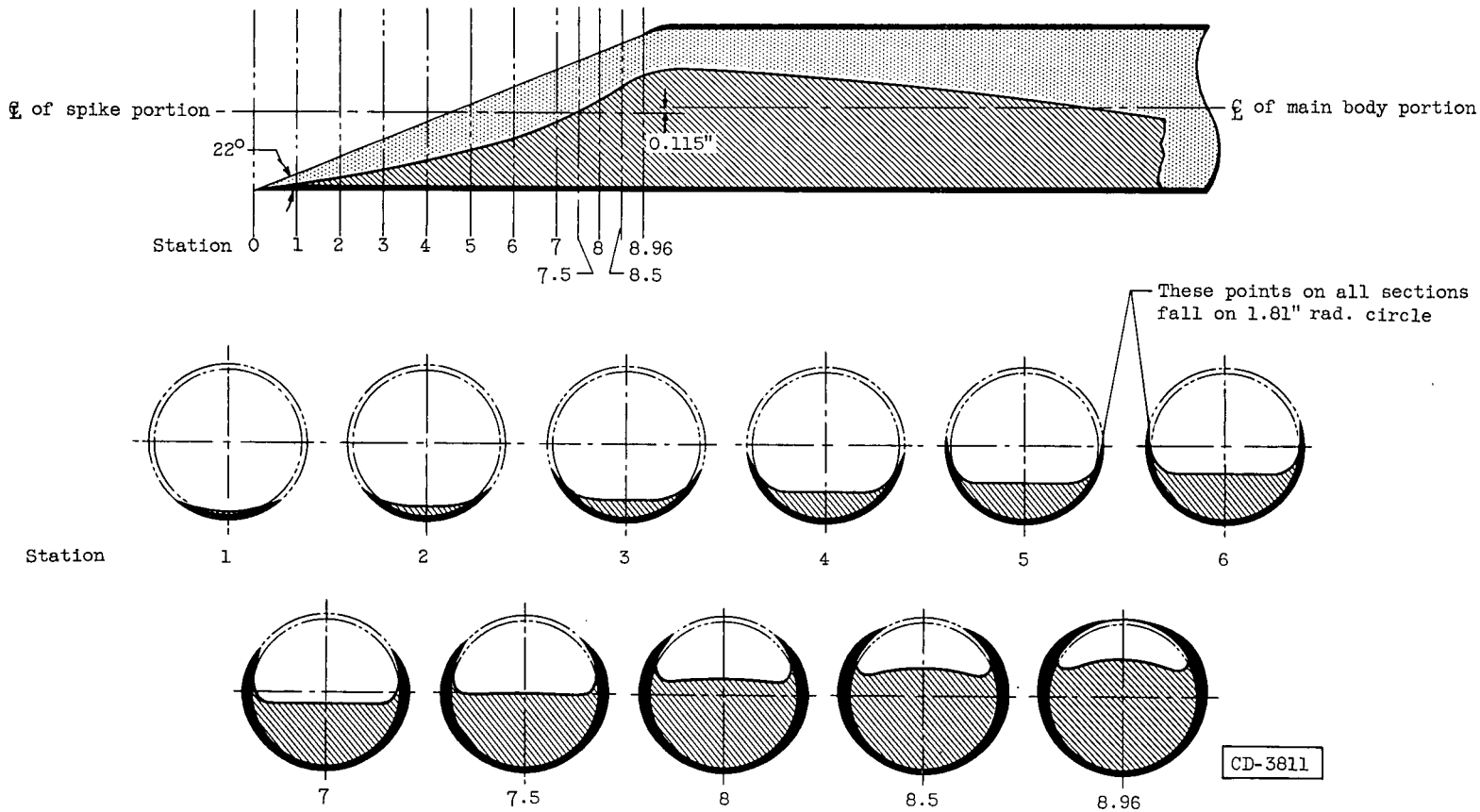

(d) Design details of asymmetric nose inlet, configuration C.

Figure 1. - Continued. Experimental apparatus.

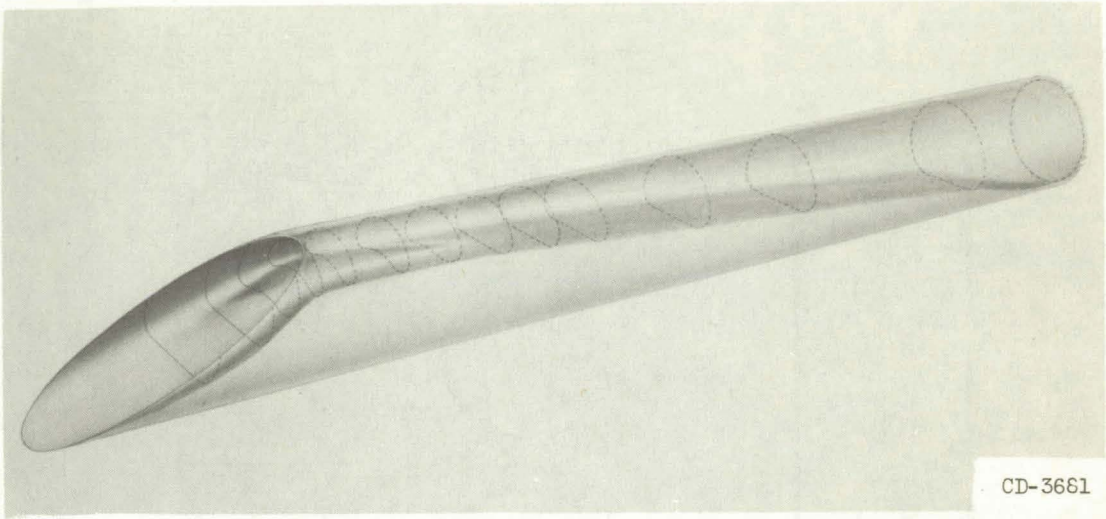

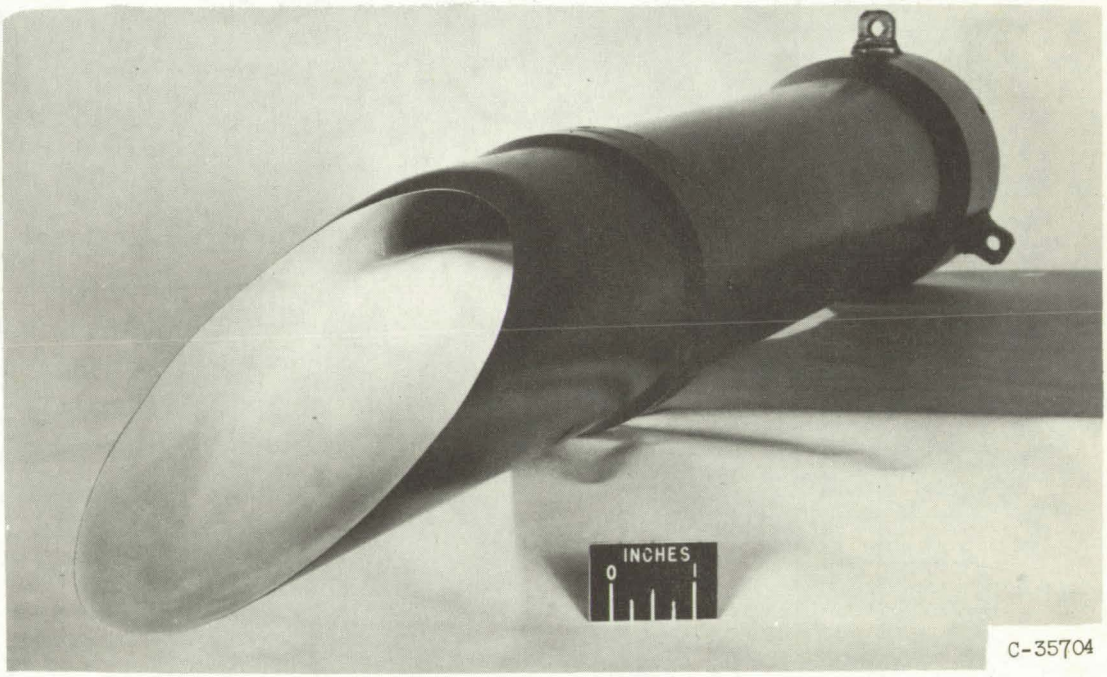

(e) Sketch and photograph of asymmetric swept nose inlet.

Figure 1. - Concluded. Experimental apparatus.

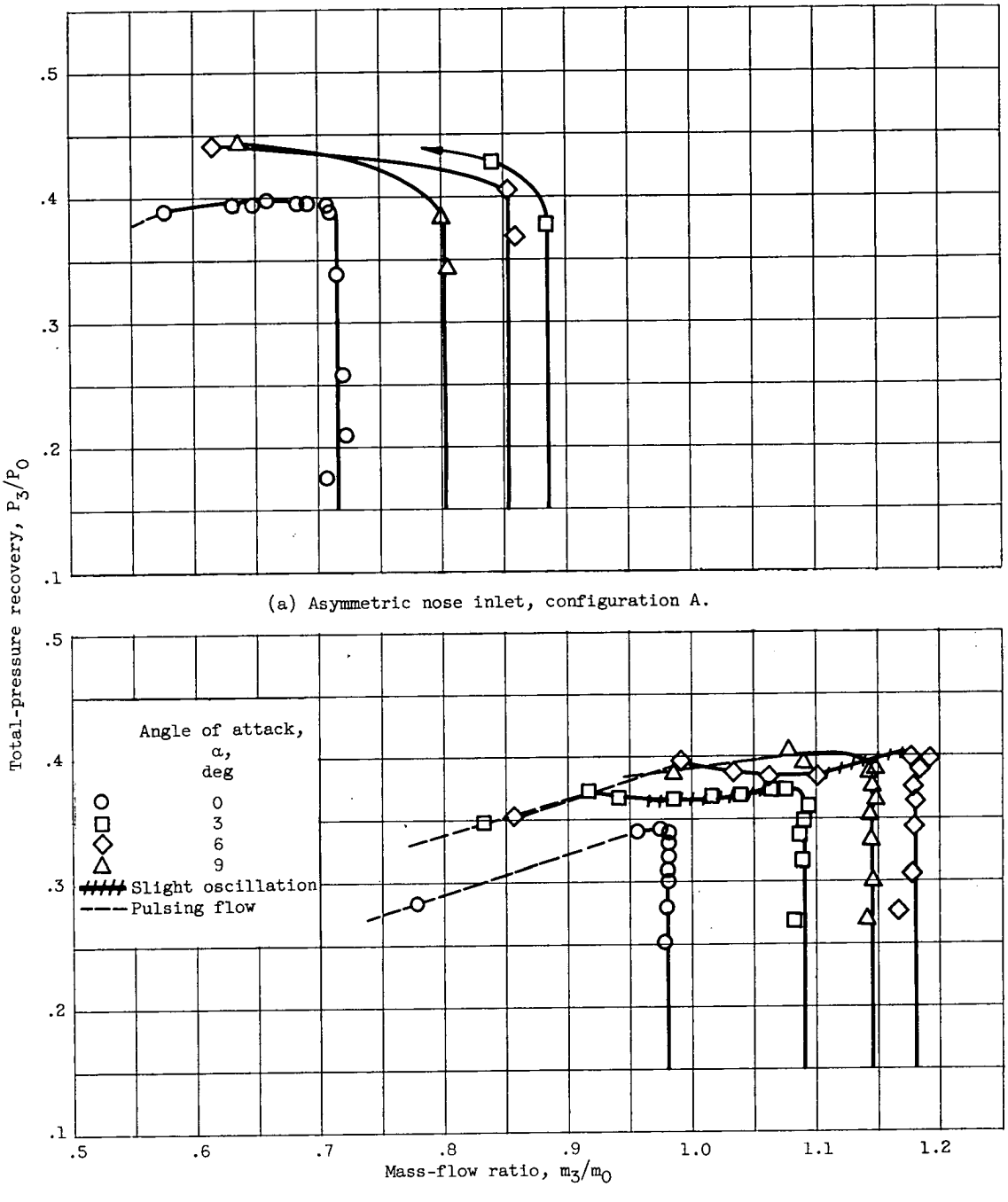

(a) Asymmetric nose inlet, configuration A.

(b) Asymmetric nose inlet, configuration B.

Figure 2. - Diffuser performance characteristics of various asymmetric inlet configurations.

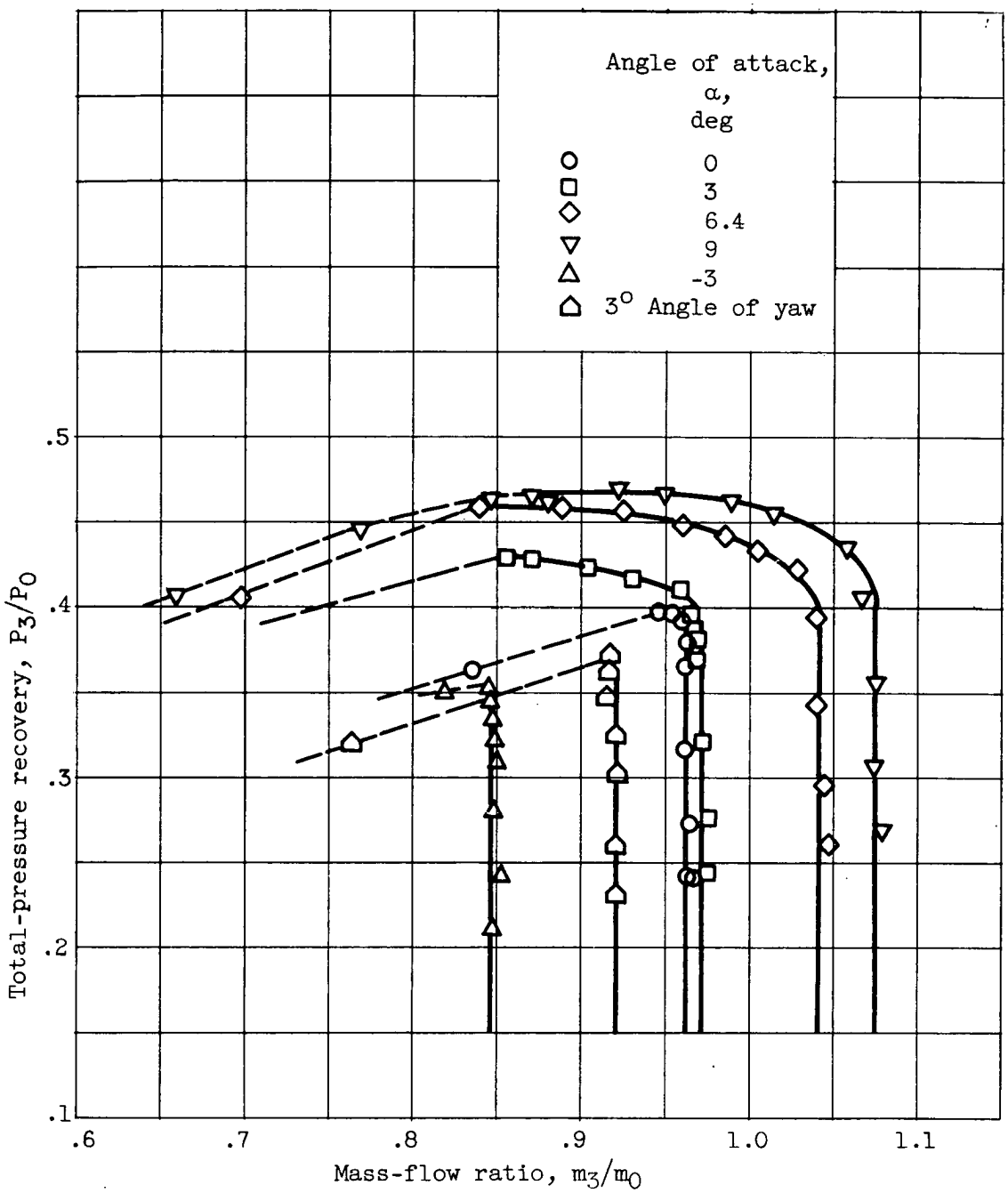

(c) Asymmetric nose inlet, configuration C.

Figure 2. - Concluded. Diffuser performance characteristics of various asymmetric inlet configurations.

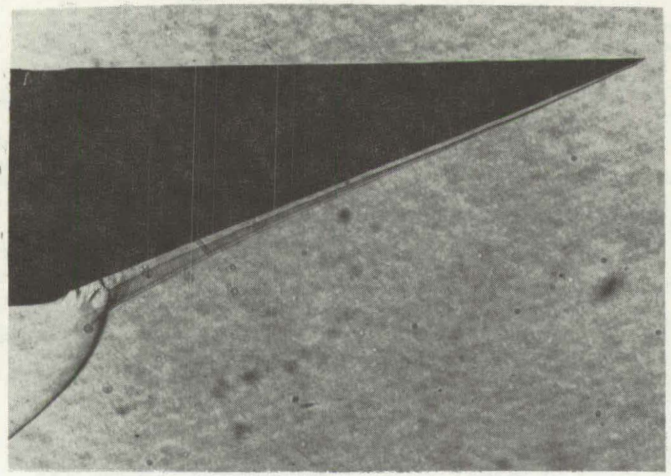

$\alpha = 0$

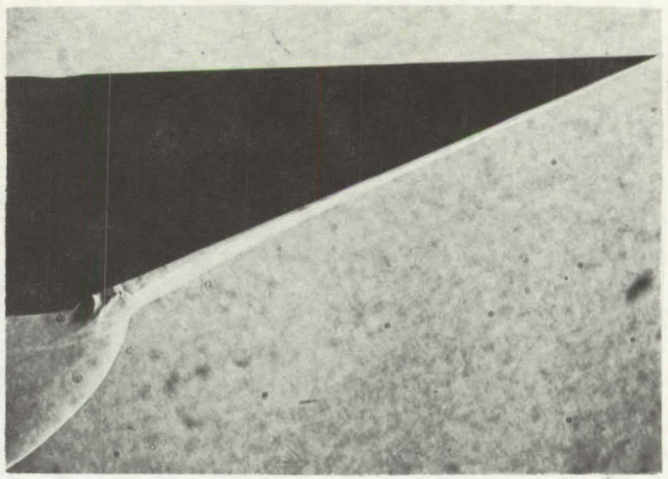

$\alpha = 3^{\circ}$

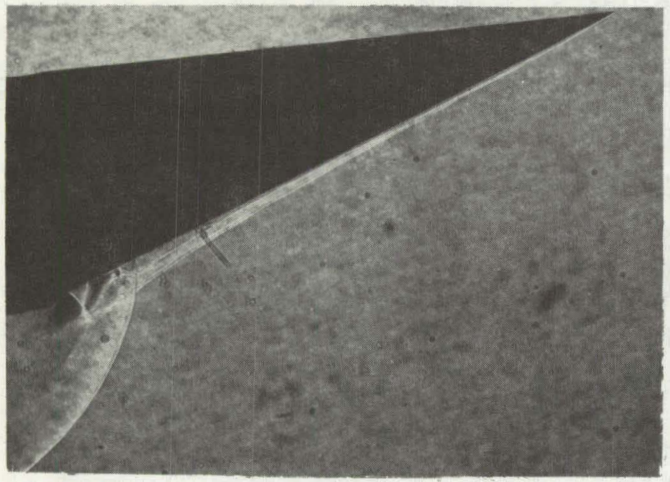

$\alpha = 6^{\circ}$

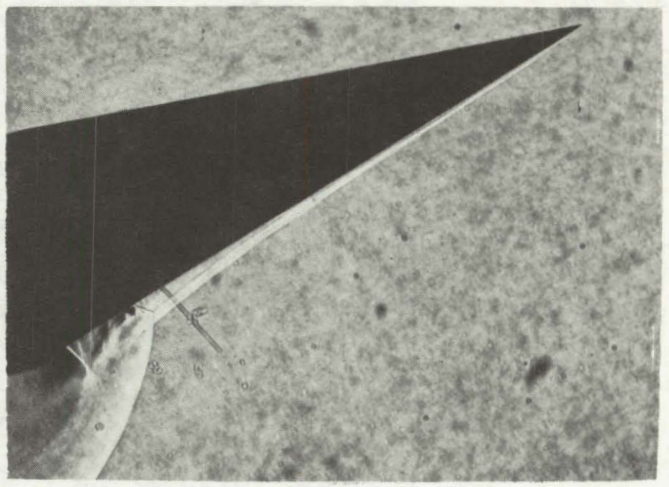

$\alpha = 9^{\circ}$ C-36376

(a) Configuration A.

Figure 3. - Supercritical flow patterns obtained with asymmetric nose inlets.

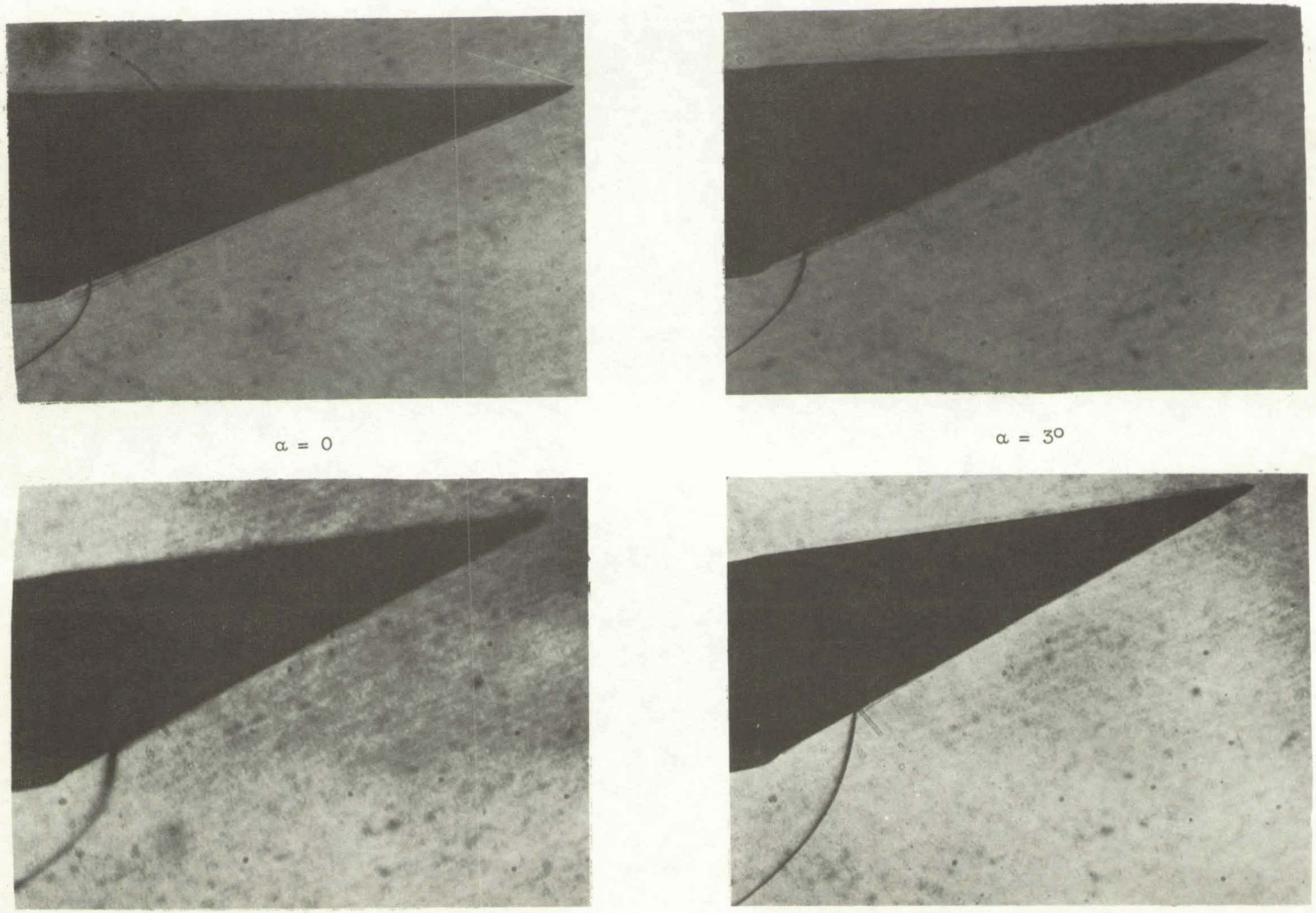

(b) Configuration B.

Figure 3. - Continued. Supercritical flow patterns obtained with asymmetric nose inlets.

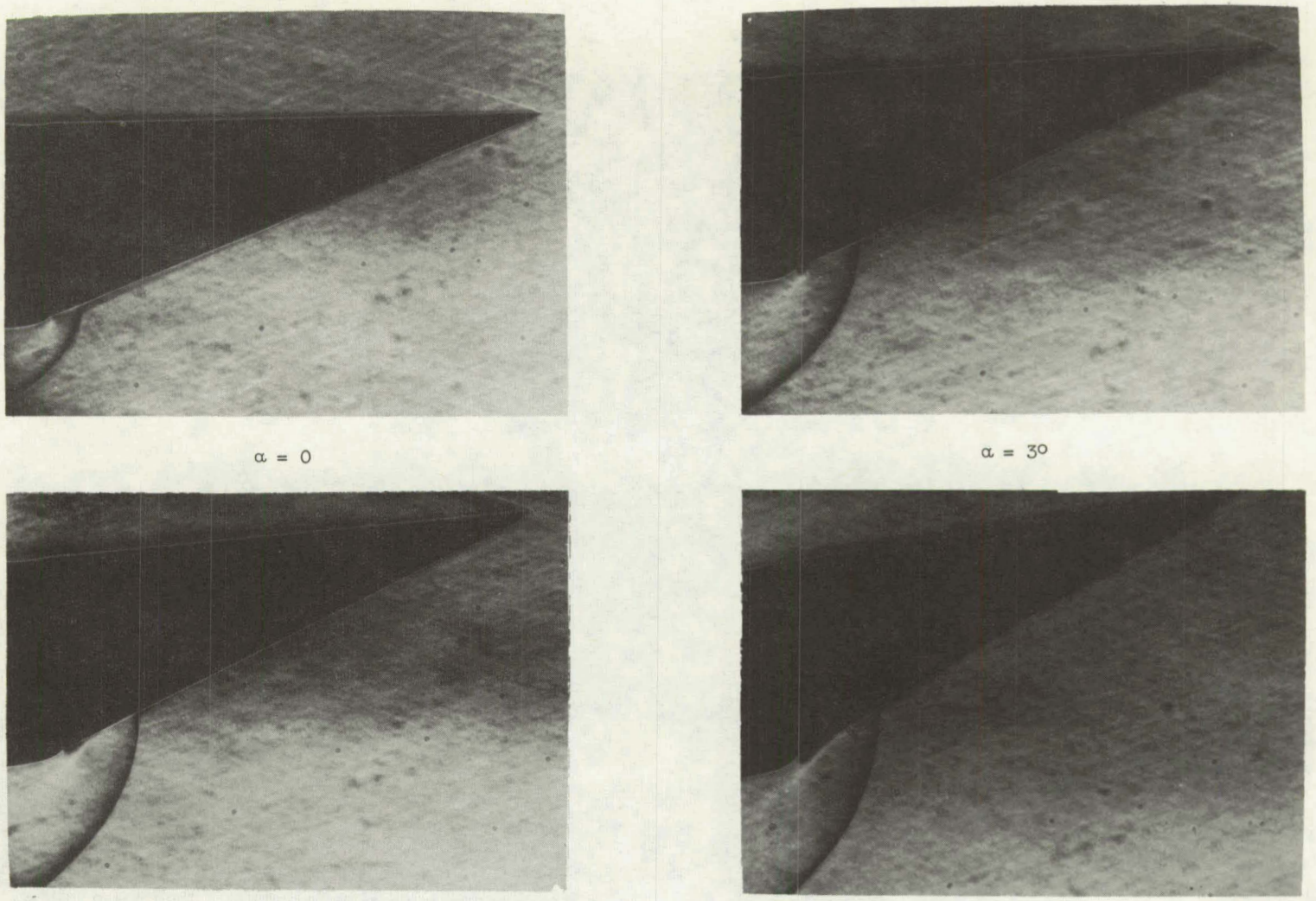

$\alpha = 0$

$\alpha = 3^\circ$

$\alpha = 6.4^\circ$

$\alpha = 9^\circ$

C-36378

(c) Configuration C.

Figure 3. - Concluded. Supercritical flow patterns obtained with asymmetric nose inlets.

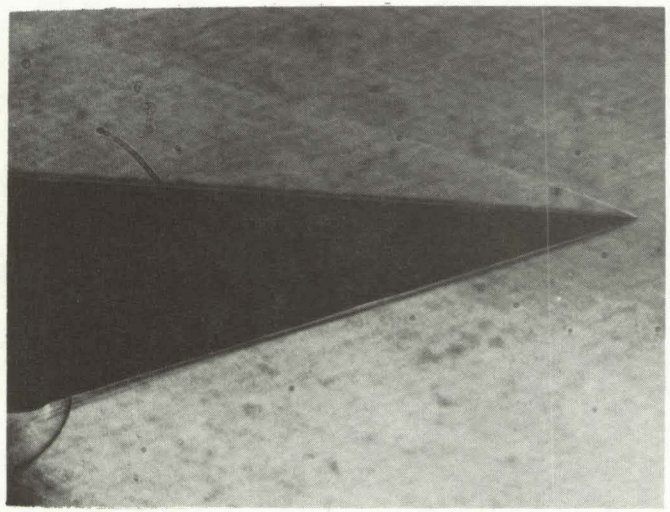

(a) Supercritical flow, -3° angle of attack

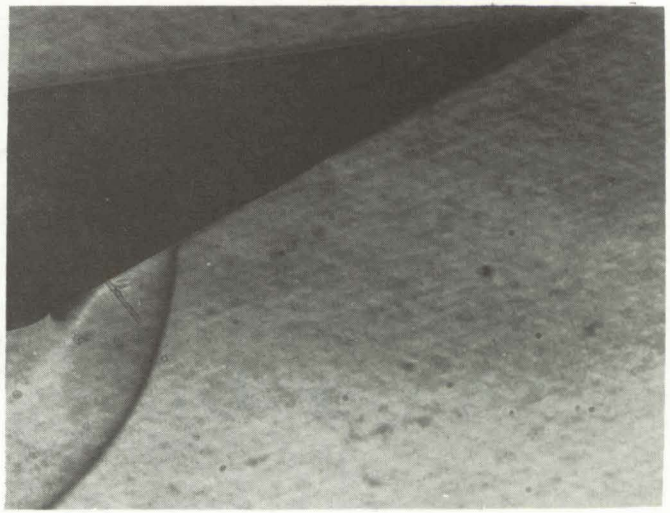

(b) Minimum stable mass flow, 9° angle of attack.

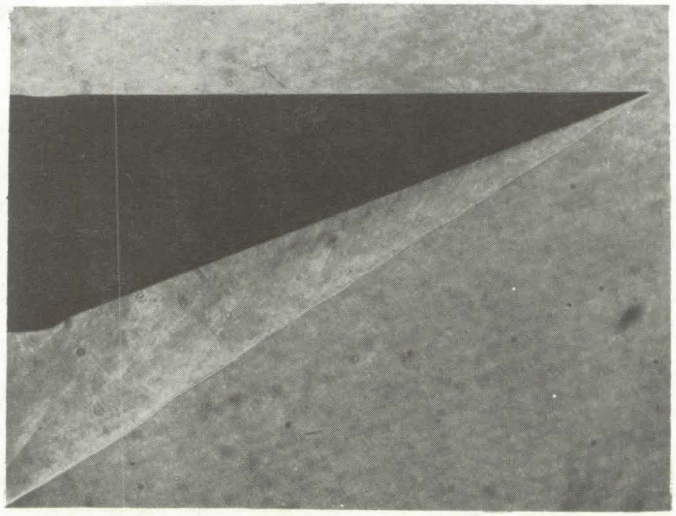

C-36379

(c) Typical buzz pattern, zero angle of attack.

Figure 4. - Additional flow patterns obtained with asymmetric inlet, configuration C.

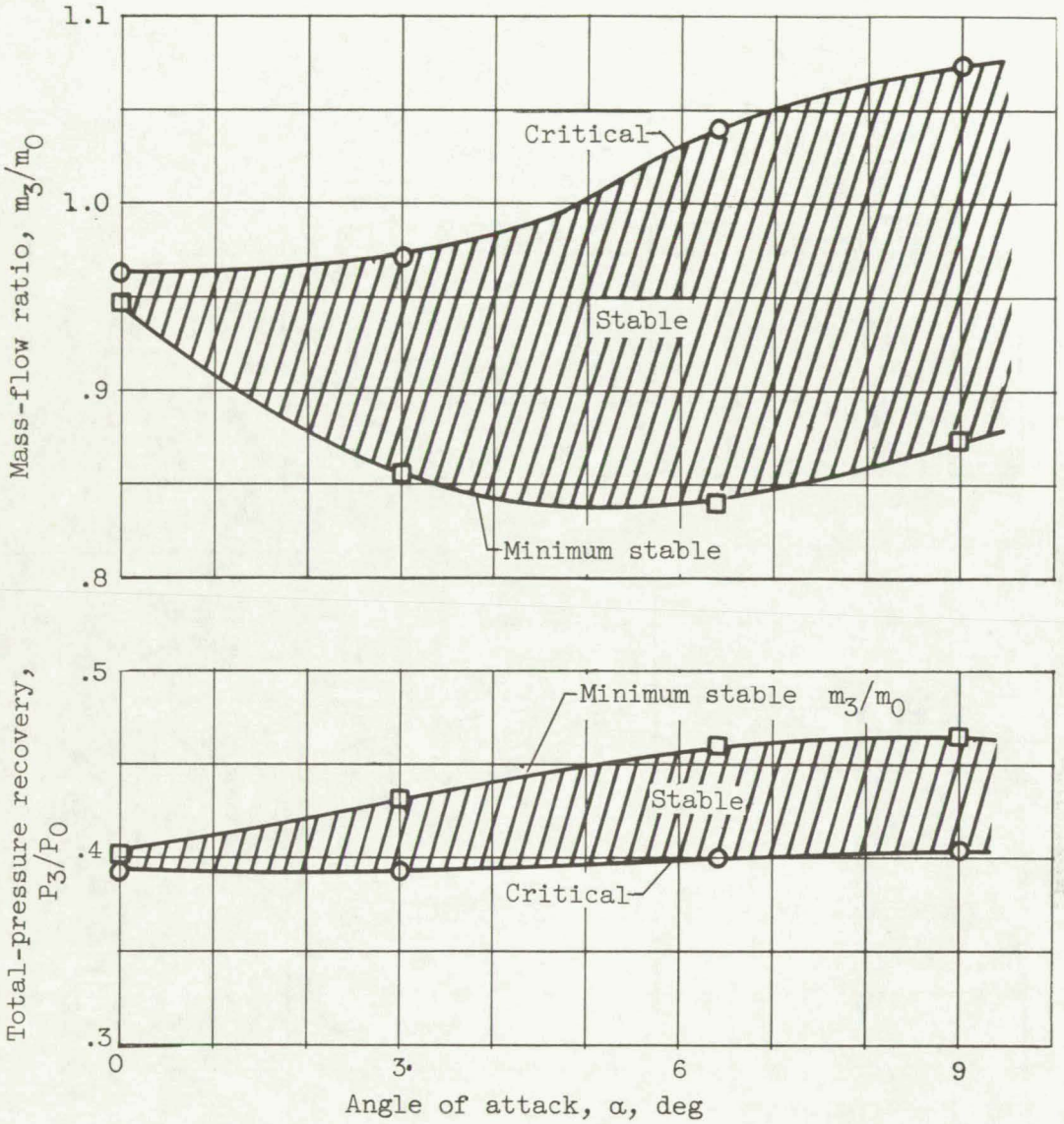

Figure 5. - Subcritical stability range obtained with asymmetric nose inlet, configuration C.

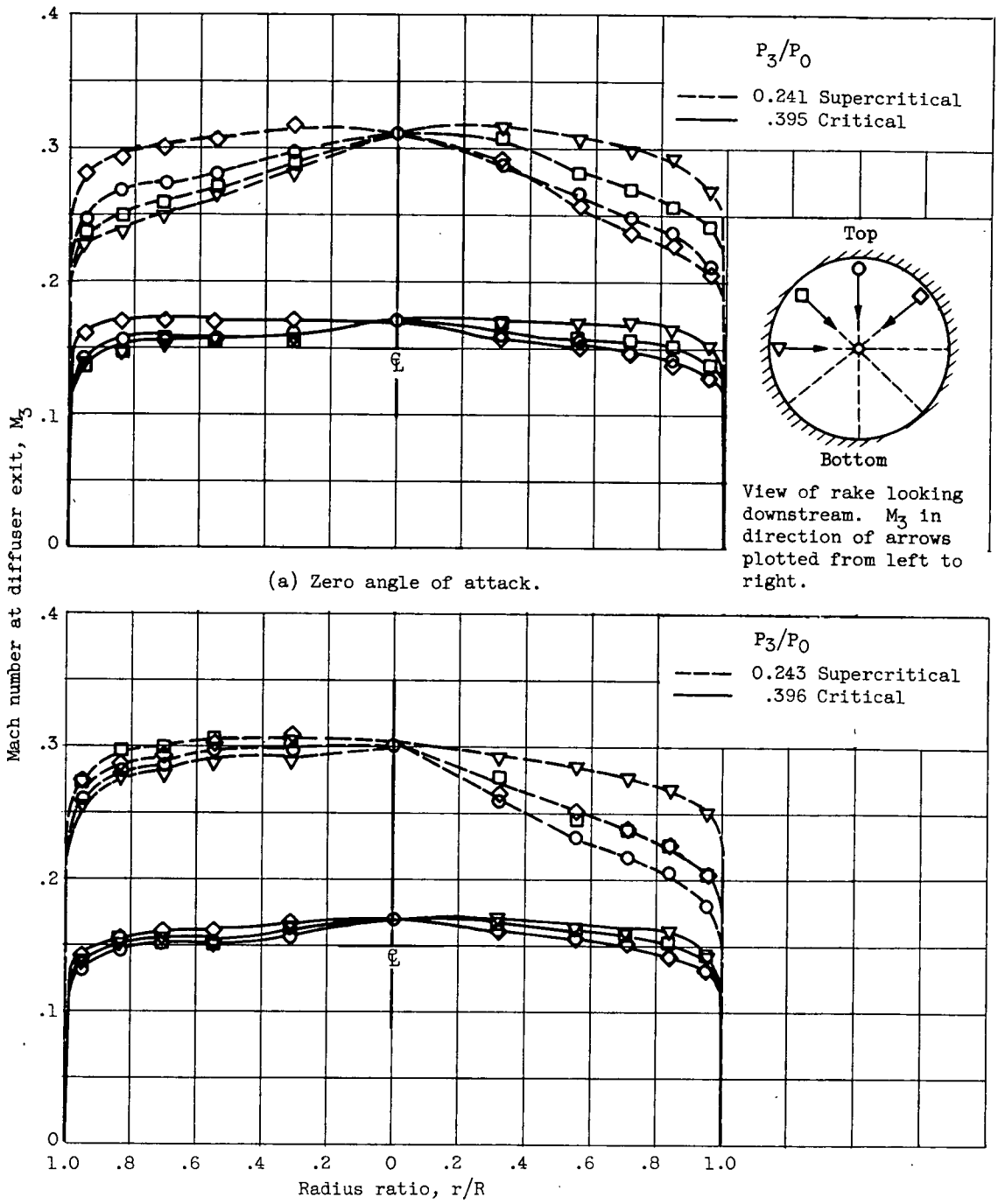

Figure 6. - Mach number profiles across diffuser exit for asymmetric nose inlet, configuration C.

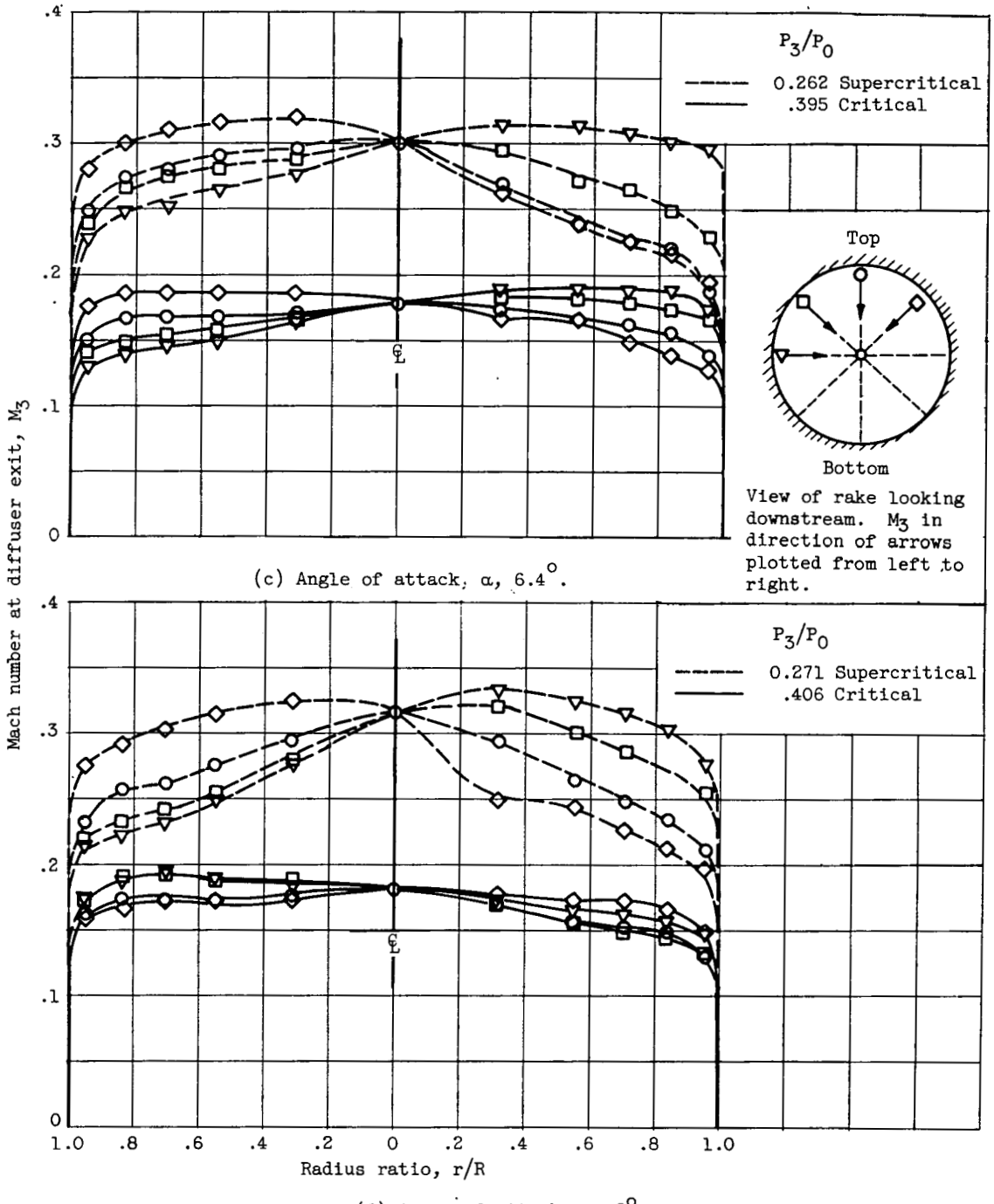

Figure 6. - Concluded. Mach number profiles across diffuser exit for asymmetric nose inlet, configuration C.

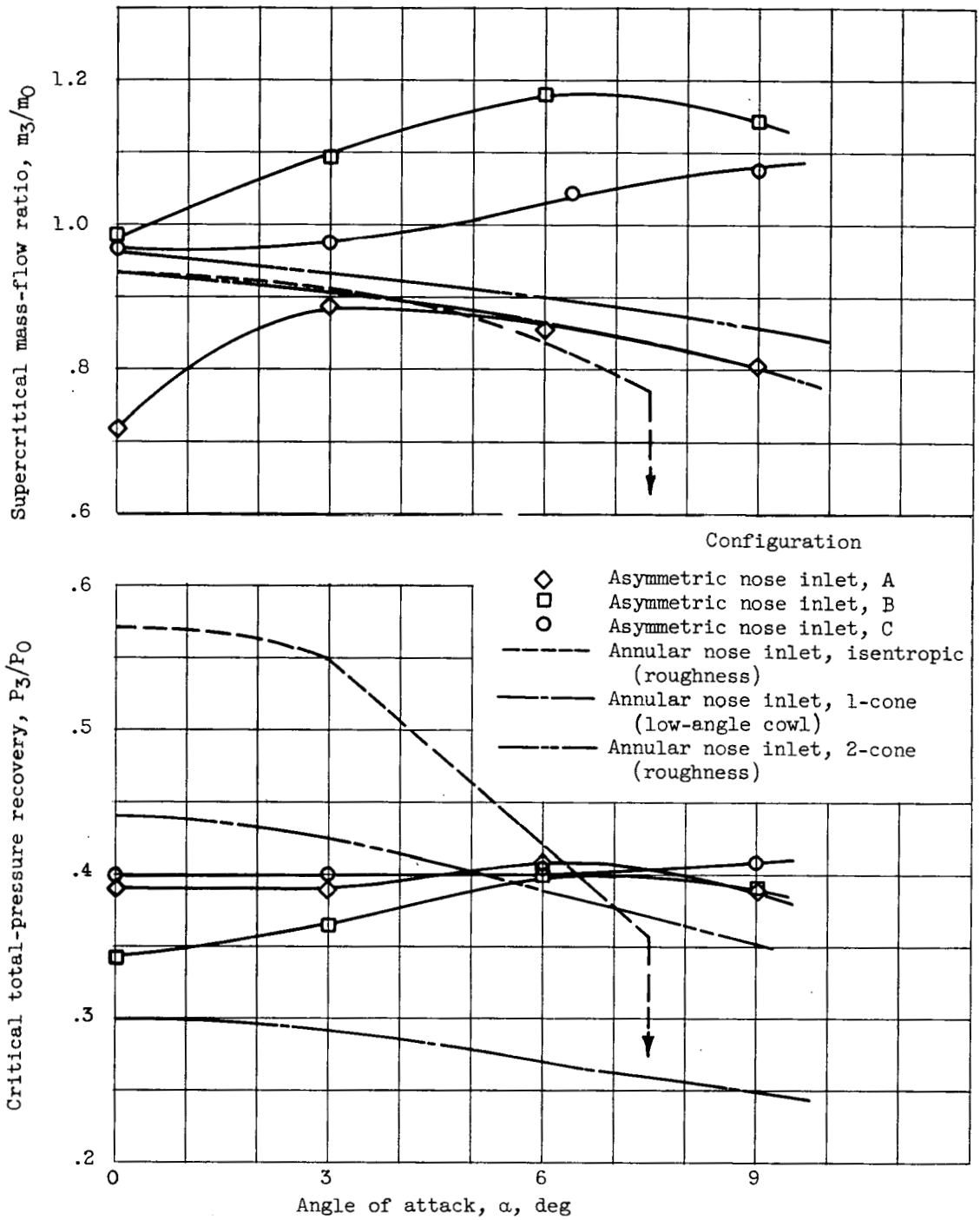

Figure 7. - Performance comparison of asymmetric nose inlets with annular nose inlets of reference 2.